

Diffusion-Aided Bandwidth-Efficient Semantic Communication with Adaptive Requests

Xuesong Wang^{*§}, Xinyan Xie[†], Mo Li^{*}, and Zhaoqian Liu^{*}
wangxuesong@cuhk.edu.cn[§]

^{*}The Chinese University of Hong Kong, Shenzhen, Shenzhen 518172, China.

[†]College of Smart Materials and Future Energy, Fudan University, Shanghai 200433, China.

Abstract—Semantic communication focuses on conveying the intrinsic meaning of data rather than its raw symbolic representation. For visual content, this paradigm shifts from traditional pixel-level transmission toward leveraging the semantic structure of images to communicate visual meaning. Existing approaches are dominated by two routes: using text-only descriptions, which typically under-specify spatial layout and fine-grained appearance details; or transmitting text alongside dense latent visual features, which can over-specify semantics and introduce redundancy and bitrate overhead. A key challenge, therefore, is to reduce semantic redundancy while preserving semantic understanding and visual fidelity, thereby improving overall transmission efficiency. This paper introduces a diffusion-based semantic communication framework with adaptive retransmission. The system transmits concise text descriptions together with a limited set of key latent visual features, and employs a diffusion-based inpainting model to reconstruct the image. A receiver-side semantic consistency mechanism is designed to evaluate the alignment between the reconstructed image and the original text description. When a semantic discrepancy is detected, the receiver triggers a retransmission to request a small set of additional latent blocks and refine the image reconstruction. This approach significantly reduces bandwidth usage while preserving high semantic accuracy, achieving an efficient balance between reconstruction quality and transmission cost.

Index Terms—Semantic communication, diffusion model, image inpainting, adaptive retransmission.

I. INTRODUCTION

Traditional communication systems aim to reliably transmit bits under channel constraints. In many scenarios, however, what ultimately matters is the utility of the received content but not exact bitwise accuracy [1]. This has motivated semantic communication, in which a transmitter conveys a representation tailored to preserve task-relevant meaning, with system performance evaluated in the task space [2], [3]. Such systems can be implemented with end-to-end neural network approaches that train encoders and decoders simultaneously, with task model optionally integrated [4], [5]. For image transmission, sending pixels demands heavy transmission bandwidth while compact semantics sustain coherent reconstructions even at low bitrate [6].

Generative models enhance this paradigm by providing a strong prior at the receiver. Latent-based diffusion models, for instance, can synthesize high-quality images using caption and/or latent as inputs, which allows transmitting latents rather than pixels to reduce bandwidth [7], [8]. However, simply

replacing pixels with latents does not fully resolve the rate bottleneck since latents still consume a significant portion of the bit budget, and text-only conditioning often results in reconstructions that diverge from the source content [9], [10]. This motivates us to propose a two-stage approach to further improve bandwidth efficiency, that is, sending a random subset of latent blocks and the caption in the first pass, and then employing feedback to request additional blocks only when necessary to improve semantic fidelity. A specially designed latent diffusion model can effectively leverage such sparse evidence by inpainting missing regions and produce a globally coherent image that aligns with available clues and the intended semantics [11], while language guidance further steers generation toward the desired content with minimal overhead [12].

This strategy naturally requires a feedback mechanism that decides when to request more blocks and when to stop. Classical hybrid ARQ uses decoder checks or CRC to trigger incremental redundancy and pursues bit-level reliability, but in semantic communication the receiver does not have the ground-truth image and bitwise correctness is not the objective, so a conventional ACK is neither available nor appropriate. Recent studies on semantic HARQ either retain a bit-level ACK and use semantic features mainly for combining or proxy triggers [13], [14], or move the decision to the task space using feature-based or topology-based detectors [15]–[17]. In this paper, we address this gap with a receiver-driven semantic acknowledgment. After each reconstruction the receiver performs caption-guided latent diffusion inpainting and generates a caption, and then compares it with the intended description using ROUGE-L (a language-based score). If the score meets a threshold the receiver issues a semantic ACK and stops transmission, otherwise it requests a small set of additional latent blocks from a reserved pool and fuses them through inpainting. This places both the trigger and the stopping rule in the semantic space and adapts the transmitted payload via feedback. It differs from prior work by using a language metric as the control signal and by coupling selective latent requests with diffusion-based inpainting, which yields substantial bandwidth savings over pixel-centric communication and full-latent decoding while maintaining stable semantic fidelity and strong visual quality.

Our contributions are twofold. First, we propose a receiver-driven semantic retransmission mechanism that uses ROUGE-

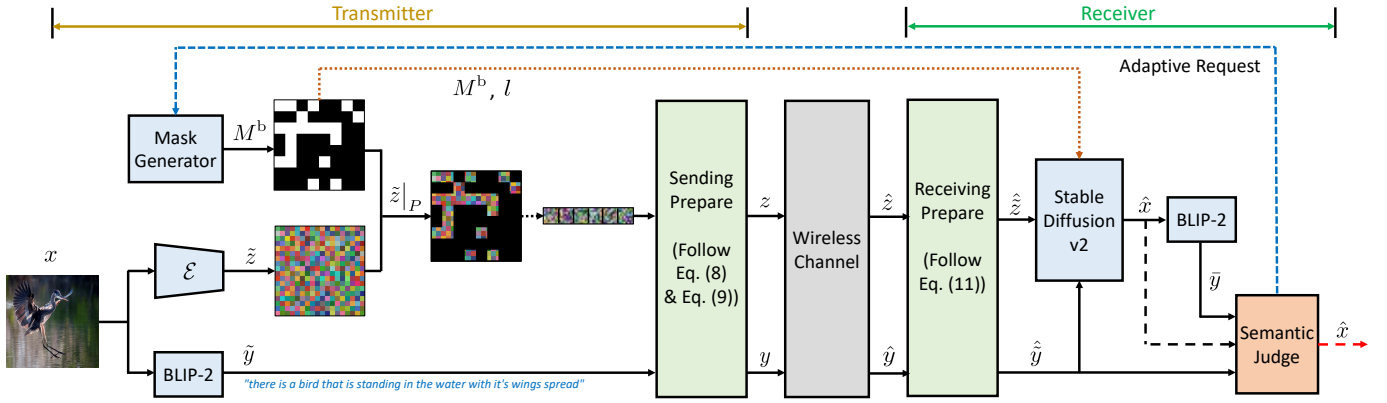


Fig. 1. Proposed system model.

L to trigger requests and to decide when to stop, aligning the control signal with task semantics. Second, we pair it with caption-guided diffusion inpainting on targeted latent blocks, enabling sparse and selective additions to produce global refinements and lower the rate while preserving semantic fidelity and visual quality.

II. SYSTEM MODEL

We consider a point-to-point image transmission system over a wireless channel. The transmitter \mathcal{T} summarizes each image as a compact latent and a short caption. The receiver \mathcal{R} reconstructs from their possibly degraded versions with a text-conditioned inpainting generator, aiming to minimize transmitted bits while preserving semantic alignment and visual fidelity.

A. Transmitter-side Design

Let $x \in \mathbb{R}^{C \times H \times W}$ denote the input image from a given dataset. A latent encoder \mathcal{E} maps x to a latent embedding

$$\tilde{z} = \mathcal{E}(x) \in \mathbb{R}^{C_L \times H_L \times W_L}. \quad (1)$$

The encoded latent is uniformly partitioned into square blocks. Given a block side length $l \in \mathbb{N}$ such that l divides both H_L and W_L , we can get

$$N_H = \frac{H_L}{l}, \quad N_W = \frac{W_L}{l}, \quad N = N_H N_W, \quad (2)$$

and index the N blocks by (i, j) with $i \in \{1, \dots, N_H\}$ and $j \in \{1, \dots, N_W\}$. Each block contains all channels, that is, block (i, j) has shape $C_L \times l \times l$. For notational simplicity, we omit the channel index C_L in what follows. All operations apply identically to every channel.

Define a binary block-level mask

$$M^b \in \{0, 1\}^{N_H \times N_W}, \quad (3)$$

where $M_{ij}^b = 0$ marks block (i, j) for transmission, and $M_{ij}^b = 1$ marks it for omission with receiver-side inpainting. Lifting the block mask to the latent spatial grid yields

$$M = M^b \otimes \mathbf{1}_{l \times l} \in \{0, 1\}^{H_L \times W_L}, \quad (4)$$

where \otimes denotes the Kronecker product and $\mathbf{1}_{l \times l}$ is the $l \times l$ all-ones matrix. Hence $M(u, v) = 0$ on transmitted regions of \tilde{z} and $M(u, v) = 1$ on withheld regions of \tilde{z} , where $u \in$

$\{1, \dots, H_L\}$ and $v \in \{1, \dots, W_L\}$. A random block mask is drawn under a prescribed withheld ratio

$$d \triangleq \frac{1}{N} \sum_{i=1}^{N_H} \sum_{j=1}^{N_W} M_{ij}^b \in [0, 1], \quad (5)$$

namely the fraction of blocks that are not transmitted, and the block-level sending rate is $q = 1 - d$. The compression ratio of x at \mathcal{T} is

$$\kappa = \frac{C_L H_L W_L}{C H W} q. \quad (6)$$

Let

$$\begin{aligned} P &= \{(i, j) : M_{ij}^b = 0\}, \\ Q &= \{(i, j) : M_{ij}^b = 1\}, \end{aligned} \quad (7)$$

be the sets of transmitted and withheld (dropped) blocks, respectively. The $M_{ij}^b = 0$ blocks are serialized and modulated into baseband symbols, given by

$$z = \mathcal{M}(\mathcal{C}(\mathcal{S}(\tilde{z}|_P))), \quad (8)$$

where $\mathcal{S}(\cdot)$ serializes the selected latent blocks into a bitstream using IEEE 754-2008 standard (64 bits per coefficient), \mathcal{C} is a rate-1/2 convolutional code, $\mathcal{M}(\cdot)$ maps bits to symbols using 16-QAM, and $\tilde{z}|_P$ denotes the collection of blocks indexed by P to be transmitted.

For the text stream, the baseband symbol sequence is obtained by applying ASCII $\mathcal{A}(\cdot)$, channel coding $\mathcal{C}(\cdot)$, and modulation $\mathcal{M}(\cdot)$ to the caption that is produced by the image-to-text converter

$$y = \mathcal{M}(\mathcal{C}(\mathcal{A}(\mathcal{F}(x)))), \quad (9)$$

where $\mathcal{F}(\cdot)$ means the image-to-text converter that produces a semantic description \tilde{y} of the image x .

The roles of z and y are asymmetric since the caption is short but semantically decisive, whereas the latent carries most of the visual detail. In the experiments we simply apply the same lightweight channel code to both streams, so that we can vary the SNR to emulate different link qualities while keeping the receiver-side reconstruction logic unchanged. Token-level noise can sharply distort meaning [18], while latent tensors are continuous and decoded by a smooth generator, so small residual distortions are visually milder than discrete-token errors [8]. Noise-aware latent handling with channel denoising

diffusion models [19] is left to future work.

Finally, both z and y are power-normalized and are sent into the same additive white Gaussian noise (AWGN) channel, given by

$$\hat{z} = z + n_z, \quad \hat{y} = y + n_y, \quad (10)$$

where $n_z, n_y \sim \mathcal{N}(0, \sigma^2 \mathbf{I})$.

B. Receiver-side Design

The receiver \mathcal{R} uses captured \hat{z} and \hat{y} to generate an image estimate \hat{x} . We assume that the block mask M^b and l are conveyed as control metadata and are assumed available to \mathcal{R} without error; M and d can be easily calculated using M^b and l . We also assume that \mathcal{R} can estimate the channel SNR accurately.

Several preparatory operations are applied to \hat{z} and \hat{y} before image reconstruction, denoted as

$$\begin{aligned} \hat{\tilde{z}} &= \oplus \left\{ \mathcal{S}^{-1} \left(\mathcal{C}^{-1} (\mathcal{M}^{-1}(\hat{z})) \right) \Big|_P; M \right\}, \\ \hat{\tilde{y}} &= \mathcal{A}^{-1} \left(\mathcal{C}^{-1} (\mathcal{M}^{-1}(\hat{y})) \right), \end{aligned} \quad (11)$$

where \mathcal{M}^{-1} , \mathcal{S}^{-1} , \mathcal{C}^{-1} and \mathcal{A}^{-1} are the inverse operations of \mathcal{M} , \mathcal{S} , \mathcal{C} and \mathcal{A} , respectively. The operator $\oplus\{\cdot; M\}$ embeds the recovered blocks into a full latent of size $C_L \times H_L \times W_L$ according to the block mask M , that is

$$[\oplus\{U; M\}](c, u, v) = \begin{cases} U(c, u, v), & \text{if } M(u, v) = 0, \\ 0, & \text{if } M(u, v) = 1, \end{cases} \quad (12)$$

where $c \in \{1, \dots, C_L\}$. That is, $\oplus\{\cdot; M\}$ places recovered values on indices with $M = 0$ and zeros elsewhere.

Next, we use a DDIM-type deterministic sampler (denoted by Γ) [20] that adopts latent diffusion inpainting to recover an estimate of \tilde{z} , that is, denoising proceeds in the latent domain while clamping the decoded blocks and updating only the masked ones. For notational simplicity, let $\tilde{z}^0 := \hat{\tilde{z}}$, and let \tilde{z}^n denote the latent at iteration n . With a text-conditioned denoiser $\epsilon_\theta(\cdot; \hat{y})$ and schedule $\bar{\alpha}_n \in (0, 1]$, the DDIM proposal (without the mask constraint) is

$$\begin{aligned} \tilde{z}_t^{n-1} &= \frac{\sqrt{\bar{\alpha}_{n-1}} \tilde{z}^n - \sqrt{1 - \bar{\alpha}_n} \epsilon_\theta(\tilde{z}^n; \hat{y})}{\sqrt{\bar{\alpha}_n}} \\ &\quad + \sqrt{1 - \bar{\alpha}_{n-1}} \epsilon_\theta(\tilde{z}^n; \hat{y}). \end{aligned} \quad (13)$$

The inpainting constraint then projects this proposal by keeping transmitted blocks fixed and updating only withheld sites:

$$\tilde{z}^{n-1} = (\mathbf{1} - M) \odot \tilde{z}_r^{n-1} + M \odot \tilde{z}_t^{n-1}, \quad (14)$$

where \tilde{z}_r^{n-1} is the decoded latent propagated to step $n-1$ by the DDIM forward map, \odot means element-wise multiplication, and $\mathbf{1}$ is an all-ones matrix matching M 's shape.

Two parameters regulate the decoder's trade-off between caption conditioning and reliance on received blocks, including a caption-guidance scale w and an inpainting strength s . w governs the weight of text conditioning relative to visual evidence from the transmitted blocks, and is held constant in our experiments. The inpainting strength s is chosen by a simple heuristic as a function of SNR (in dB) and d , decreasing

Algorithm 1 Receiver-side semantic-driven adaptive retransmission.

Require: \hat{z}, \hat{y}, M^b, l .

- 1: derive P_0, Q_0 from Eq. (7) and M from Eq. (4).
 - 2: compute $\tilde{z}^0 := \hat{\tilde{z}}, \hat{\tilde{y}}$ from Eq. (11).
 - 3: set $t \leftarrow 0, P_t \leftarrow P_0, Q_t \leftarrow Q_0, \tilde{z}_t^0 \leftarrow \tilde{z}^0$.
 - 4: **repeat**
 - 5: $(M_t^b)_{ij} \leftarrow \mathbb{1}\{(i, j) \in Q_t\}; M_t \leftarrow M_t^b \otimes \mathbf{1}_{l \times l}$.
 - 6: $\hat{\tilde{z}}_t \leftarrow \oplus \left\{ \mathcal{S}^{-1} (\mathcal{C}^{-1} (\mathcal{M}^{-1}(\hat{\tilde{z}}))) \Big|_{P_t}; M_t \right\}; \tilde{z}_t^0 \leftarrow \hat{\tilde{z}}_t$.
 - 7: $d_t \leftarrow |Q_t|/N; s_t \leftarrow s(\text{SNR}, d_t); S_t \leftarrow \lceil s_t T \rceil$.
 - 8: **for** $\gamma \in \{w, 0\}$ **do**
 - 9: $\hat{x}_t^{(\gamma)} \leftarrow \Gamma(\tilde{z}_t^0, M_t; \gamma, s_t, S_t);$
 - 10: $\bar{y}_t^{(\gamma)} \leftarrow \mathcal{F}(\hat{x}_t^{(\gamma)}); r_t^{(\gamma)} \leftarrow \Phi(\bar{y}_t^{(\gamma)}, \hat{y});$
 - 11: **end for**
 - 12: select $r_t = \max\{r_t^{(w)}, r_t^{(0)}\}$ and the corresponding \hat{x}_t .
 - 13: **if** $r_t < \tau$ **and** $t < t_{\max}$ **then**
 - 14: choose $\Delta_t \subseteq Q_t$ uniformly with $|\Delta_t| = \rho N$ and request Δ_t .
 - 15: $P_{t+1} \leftarrow P_t \cup \Delta_t; Q_{t+1} \leftarrow Q_t \setminus \Delta_t; t \leftarrow t + 1$.
 - 16: **end if**
 - 17: **until** $r_t \geq \tau$ **or** $t = t_{\max}$
 - 18: **return** \hat{x}_t
-

with larger SNR and increasing with larger d . Operationally, a larger s both intensifies masked-region updates and maps to a larger number of DDIM steps. The DDIM inpainting trajectory proceeds from iteration $n = \lceil sT \rceil$ to $n = 0$ under the update above, where T is the maximum step of diffusion sampler Γ . After reaching \tilde{z}^0 , the VAE decoder \mathcal{D} maps the final latent to the reconstructed image \hat{x} .

C. Adaptive Retransmission with Receiver-side Semantic Criterion

Deciding in advance how many latent blocks to send is difficult, because the useful evidence depends on image content and channel conditions. We adopt a receiver-driven semantic retransmission mechanism in which both the trigger and the stopping rule are defined in the semantic space to match the communication objective. Since the original image is unavailable at the receiver, we use ROUGE-L [21] (denoted by Φ) to score the reconstruction by generating a caption $\bar{y} = \mathcal{F}(\hat{x})$ and computing $r = \Phi(\bar{y}, \hat{y}) \in [0, 1]$. Larger r indicates stronger semantic alignment between the reconstruction and the received intent. If r exceeds the threshold τ , the session terminates. Otherwise the receiver requests a small number of withheld latent blocks uniformly at random, merges them with the received set, and updates the mask using the indicator function $\mathbb{1}(\cdot)$ to define the next inpainting region.

Let P_0 and Q_0 be the initial transmitted and withheld index sets that are obtained from M^b , with round index 0 as their lower subscript and $|P_0| + |Q_0| = N$. At round t , the receiver requests a subset $\Delta_t \subseteq Q_t$ with $|\Delta_t| = \rho N$, where ρ is the per-round budget ratio. The sets update as

$$Q_{t+1} = Q_t \setminus \Delta_t, \quad P_{t+1} = P_t \cup \Delta_t, \quad (15)$$

where $t \in \mathbb{N}$ and $t \leq t_{\max}$. Only newly requested blocks are transmitted. In each round, the decoder reruns with the calculated strength s . Guidance is used as an optional enhancement in which the decoder selects the image corresponding to the highest r_t . Algorithm 1 summarizes the receiver-side semantic-driven adaptive retransmission in our system.

Remarks. We do not model packet erasures in the present system, and we assume the request link is reliable and negligible. These extensions are left to future work.

III. EXPERIMENTS AND RESULTS

In this section, we first introduce the simulation setting in our experiments, and describe the metrics that are used to evaluate the system performance. Then we show the results generated by our proposed system and discuss them in detail.

A. Simulation Settings and Benchmarks

We use Stable Diffusion v2.1 as the generative backbone and BLIP-2 as the receiver-side captioner (referring to Γ and \mathcal{F} in Algorithm 1). Stable Diffusion v2.1 provides latent-diffusion inpainting to reconstruct images from partial latent evidence plus text guidance, while BLIP-2 generates candidate captions used by the receiver to assess semantic alignment via ROUGE-L. Experiments are conducted on Flickr30k dataset. Each image is resized then encoded by the Stable Diffusion v2.1 VAE (variational autoencoder) encoder. After dividing the latent into blocks, the transmission follows a per-round budget capping the overall rate at no more than 0.5.

To comprehensively evaluate system performance, beyond using ROUGE-L as the receiver-side semantic criterion, we adopt complementary metrics that capture different facets of reconstruction quality. SSIM assesses pixel-level fidelity (higher is better). LPIPS measures perceptual dissimilarity as a distance in deep feature space (lower is better). FID quantifies distributional realism by fitting Gaussians to Inception-V3 feature embeddings of generated and reference image sets and computing their Fréchet distance (lower is better). Finally, CLIP-IT measures image-text semantic alignment as the cosine similarity between CLIP image and text embeddings (higher is better).

For comparison, we evaluate the following configurations in addition to the main scheme:

- No-guidance scheme, in which y is not transmitted from \mathcal{T} , and \mathcal{R} reconstructs the image without text conditioning.
- Full-mask scheme, in which \mathcal{T} sends only y but no latent blocks to \mathcal{R} , equivalent to $M^b = 1$.

Note that the inpainting strength s in Algorithm 1 is set by the heuristic method in Table I. Within the experimental range $\text{SNR} \in [5, 10]$ and drop ratio $d \in [0.5, 0.875]$, it yields $s \in [0.707, 1]$, increasing with larger d and decreasing as SNR improves. For a fair comparison, both the no-guidance and full-mask baselines use the same s as the main scheme. The no-guidance baseline further adopts the same mask schedule as the main scheme (thus performs the same number of rounds t as main scheme), while the full-mask baseline corresponds

TABLE I
KEY SIMULATION SETTINGS.

Image size	$3 \times 512 \times 512$
Latent size	$4 \times 64 \times 64$
Block size on latent grid	$l \in \{4, 8\}$
First pass sending rate	$q_0 = 0.125$
Per-round budget	$\rho = 0.0625$
Channel model	AWGN channel; SNR $\in [5, 10]$ dB
Guidance scale	$w = 9$ (fixed)
Inpainting strength	$s = \min\{1, \sqrt{d}(1 - 0.1 \tanh(\text{SNR} - 10))\}$
DDIM maximum steps	$T = 50$
Max rounds	$t_{\max} = 6$

to $t = 0$ with caption-only conditioning. We intentionally exclude the no-mask scheme that transmits all latent blocks, because it constitutes an unconstrained upper bound rather than a comparable baseline, and its advantage reflects rate rather than algorithmic effects.

Here we clarify rate accounting in different schemes. With the caption length capped at 40 tokens, the generated string contains about 60 to 100 characters, which is about 960 to 1600 bits per sentence after serializing and channel coding. By contrast, one request of latent blocks carries 131072 bits, so the text contributes only a very small fraction of the transmitted bits and does not obviously bias comparisons with the no-guidance scheme. Note that this is on top of compressing the image into latent space, and the adaptive scheme still sends less than transmitting the whole latent.

B. Experiment Results and Discussions

Fig. 2 studies the effect of the ROUGE-L threshold τ on the adaptive loop over all SNR values. As τ increases, the system becomes more conservative in stopping, which raises the total number of transmissions t by allocating additional retransmission rounds beyond the first pass. Correspondingly, the overall compression ratio κ increases with τ while the drop rate d decreases, reflecting that stricter semantic consistency induces the receiver to request more latent evidence. The round-wise histogram further shows that small τ concentrates terminations in the first one or two rounds, whereas large τ shifts mass to later rounds; nevertheless, most sessions still finish within a small t because inpainting effectively propagates sparse evidence across the masked regions. This validates that τ acts as a direct semantic knob on the rate-fidelity tradeoff, where lower τ yields aggressive savings through earlier stops and higher τ spends more bits to drive stronger agreement with the intended description.

Fig. 3(a)-(d) demonstrate system performance under $\tau = 0.7$ for two l sizes, comparing the main scheme with the no-guidance scheme. ROUGE-L in Fig. 3(a) remains highest for the main scheme across SNR values, and is relatively insensitive to channel quality. CLIP-IT in Fig. 3(b) also favors the main scheme with small fluctuations over SNR, and prefers $l = 8$ over $l = 4$ under the main scheme, suggesting that coarser blocks convey more coherent mid-level structure per request that benefits cross-modal matching. On pixel and perceptual metrics, the pattern partly reverses. For SSIM in Fig. 3(c), the main scheme is slightly higher than no-guidance when $l = 4$, but slightly lower when $l = 8$. For LPIPS in

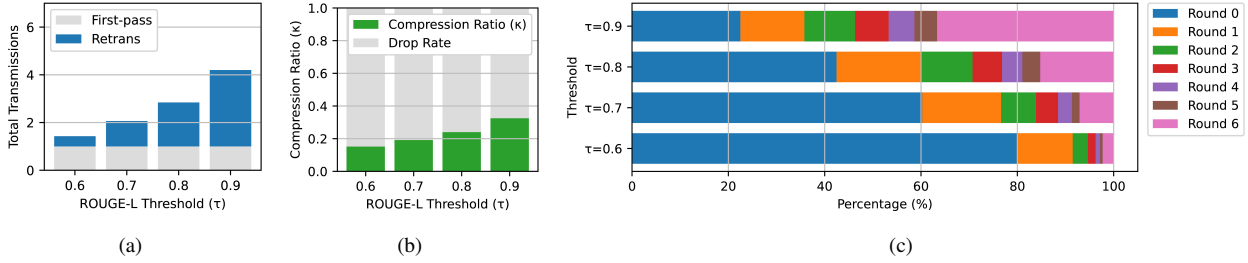


Fig. 2. System performance over different τ values. (a) Total transmission rounds t . (b) Compression ratio κ . (c) Round-wise histogram.

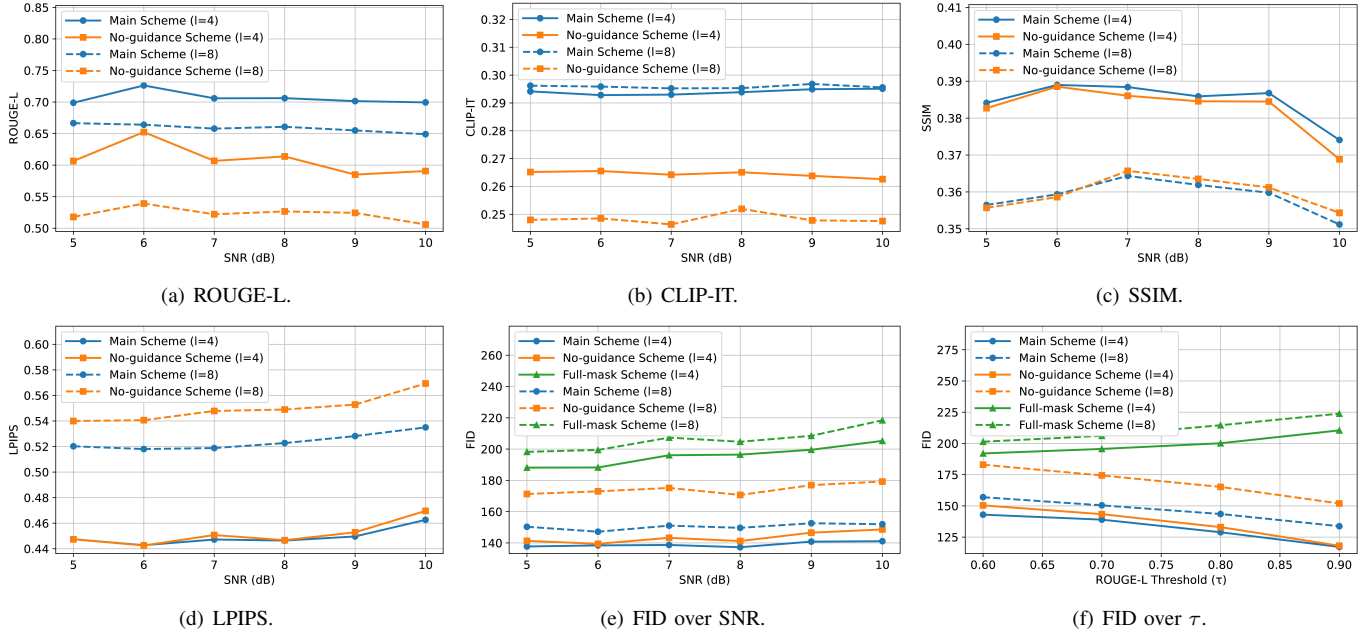


Fig. 3. System average performance. (a)(b)(c)(d) metrics over SNR values at $\tau = 0.7$. (e)(f) FID performance over SNR and τ values.

Fig. 3(d), the two methods are nearly identical when $l = 4$, while the main scheme is clearly better when $l = 8$ because lower LPIPS is preferred. Both SSIM and LPIPS show that $l = 4$ performs better than $l = 8$, and both slightly worsen as SNR increases. These trends are consistent with a semantic-pixel tradeoff. Caption guidance steers inpainting toward text-aligned content and perceptual coherence, which improves LPIPS values, and it can reduce local pixel agreement in some settings, which affects SSIM and is more pronounced with coarser blocks ($l = 8$). Finer blocks enable more targeted fixes that improve local structure and texture statistics, which explains the advantage of $l = 4$ for SSIM and LPIPS, even when cross-modal alignment prefers $l = 8$ in CLIP-IT. The mild degradation of SSIM and the slight rise in LPIPS with increasing SNR can be explained by the stopping rule. At higher SNR the receiver reaches the ROUGE-L threshold earlier and requests fewer additional blocks, leading to less latent evidence and fewer denoising steps. As a result, pixel-level and perceptual gains are slightly smaller while semantic alignment remains stable.

Fig. 3(e) and (f) analyze distributional realism using FID. In Fig. 3(e), FID becomes slightly worse as SNR increases for all configurations, which is consistent with earlier stopping

at high SNR that reduces the amount of corrective evidence the receiver acquires. In Fig. 3(f), increasing the threshold τ clearly improves FID in our main scheme, since higher τ triggers additional requests that carry useful information, with diminishing returns at large τ comparing to the no-guidance scheme. In both subfigures $l = 4$ is better than $l = 8$, which suggests that finer grained additions align global feature statistics more effectively even when CLIP-IT prefers coarser blocks. Taken together, these results show that the semantic controller yields stable language-level alignment across channels, while the choice of l trades cross-modal alignment (which favors $l = 8$) against local and distributional fidelity (which favors $l = 4$). Adjusting τ tunes the balance between realism and rate, with higher τ improving realism at the expense of more rounds t and lower τ reducing the number of rounds t and the rate.

Fig. 4 depicts qualitative reconstructions under three compression ratios. Within each row, the caption-only full-mask baseline produces globally plausible but semantically unstable images, with noticeable losses of fine structure at all budgets. The no-guidance scheme tends to preserve local textures more faithfully, yielding higher pixel similarity but exhibiting semantic drift in content and layout, especially at lower budgets.



Fig. 4. Reconstructions at termination for sessions with final compression ratio (a) $\kappa = 0.125$, (b) $\kappa = 0.25$, (c) $\kappa = 0.375$, under SNR 7 dB, $l = 4$ and $\tau = 0.7$. Columns from left to right: original images, full-mask scheme, no-guidance scheme, main scheme.

In contrast, the proposed main scheme restores the intended semantics more reliably while maintaining coherent appearance; at $\kappa = 0.125$ it already corrects notable mismatches relative to the no-guidance scheme, and as κ increases to 0.25 and 0.375, a few retransmissions progressively resolve residual inconsistencies without resorting to dense transmission. These visual trends are consistent with the quantitative results, as semantic guidance trades a small amount of pixel-level accuracy for stronger alignment with the intended description and larger κ tightens both semantic and perceptual fidelity across methods.

Finally, we present a brief complexity note. The total compute scales with the sum of denoising steps executed across rounds in the latent diffusion sampler. VAE encode and decode and ROUGE-L scoring add only small overheads relative to denoising. Memory is dominated by U-Net activations and model parameters and remains essentially constant across rounds. In our setup with an RTX 5080 GPU with an AMD 9700X CPU, single-image inference completes in under three seconds.

IV. CONCLUSION

This paper presents a receiver-driven semantic retransmission framework that sends a short caption with a sparse set of latent blocks at the transmitter, and reconstructs images by caption-guided diffusion inpainting at the receiver. A language-based score drives the loop, so the receiver requests additional latent blocks only when the semantic criterion is not met. This strategy aligns the control signal with semantics, reduces the first-pass payload, and spends extra bits where they provide the largest semantic gain. Experiments show substantial bandwidth savings over pixel-based and dense latent baselines while maintaining stable ROUGE-L and consistent perceptual quality. We also observe a trade-off between block size and semantic fidelity, and a balance between image reconstruction and rate control by tuning the threshold. Future work includes learning a block selection policy, modeling reliability for text and latent streams, and extending the framework to video and multi-user scenarios.

REFERENCES

- [1] Y. E. Sagduyu, S. Ulukus, and A. Yener, "Task-oriented communications for NextG: End-to-end deep learning and AI security aspects," *IEEE Wireless Communications*, vol. 30, no. 3, pp. 52–60, 2023.
- [2] Y. Liu, X. Wang, Z. Ning, M. Zhou, L. Guo, and B. Jedari, "A survey on semantic communications: technologies, solutions, applications and challenges," *Digital Communications and Networks*, vol. 10, no. 3, pp. 528–545, 2024.
- [3] X. Wang, M. Li, X. Shi, Z. Liu, and S. Yang, "Diffusion-based Task-oriented Semantic Communications with Model Inversion Attack," *arXiv preprint arXiv:2506.19886*, 2025.
- [4] C. Liu, C. Guo, Y. Yang, W. Ni, Y. Zhou, L. Li, and T. Q. Quek, "Explainable semantic communication for text tasks," *IEEE Internet of Things Journal*, 2024.
- [5] E. Grassucci, S. Barbarossa, and D. Comminiello, "Generative semantic communication: Diffusion models beyond bit recovery," *arXiv preprint arXiv:2306.04321*, 2023.
- [6] T.-Y. Tung, H. Esfahanizadeh, J. Du, and H. Viswanathan, "Multi-level reliability interface for semantic communications over wireless networks," *IEEE Transactions on Communications*, 2025.
- [7] A. Blattmann, R. Rombach, H. Ling, T. Dockhorn, S. W. Kim, S. Fidler, and K. Kreis, "Align your latents: High-resolution video synthesis with latent diffusion models," in *Proceedings of the IEEE/CVF conference on computer vision and pattern recognition*, 2023, pp. 22 563–22 575.
- [8] R. Rombach, A. Blattmann, D. Lorenz, P. Esser, and B. Ommer, "High-resolution image synthesis with latent diffusion models," in *Proceedings of the IEEE/CVF conference on computer vision and pattern recognition*, 2022, pp. 10 684–10 695.
- [9] G. Cicchetti, E. Grassucci, J. Park, J. Choi, S. Barbarossa, and D. Comminiello, "Language-oriented semantic latent representation for image transmission," in *2024 IEEE 34th International Workshop on Machine Learning for Signal Processing (MLSP)*. IEEE, 2024, pp. 1–6.
- [10] X. Wang, D. Ye, C. Feng, H. H. Yang, X. Chen, and T. Q. Quek, "Trustworthy image semantic communication with GenAI: Explainability, controllability, and efficiency," *IEEE Wireless Communications*, vol. 32, no. 2, pp. 68–75, 2025.
- [11] S. Xie, Z. Zhang, Z. Lin, T. Hinz, and K. Zhang, "Smartbrush: Text and shape guided object inpainting with diffusion model," in *Proceedings of the IEEE/CVF conference on computer vision and pattern recognition*, 2023, pp. 22 428–22 437.
- [12] H. Manukyan, A. Sargsyan, B. Atanyan, Z. Wang, S. Navasardyan, and H. Shi, "Hd-painter: high-resolution and prompt-faithful text-guided image inpainting with diffusion models," in *The Thirteenth International Conference on Learning Representations*, 2023.
- [13] Q. Zhou, R. Li, Z. Zhao, Y. Xiao, and H. Zhang, "Adaptive bit rate control in semantic communication with incremental knowledge-based HARQ," *IEEE Open Journal of the Communications Society*, vol. 3, pp. 1076–1089, 2022.
- [14] H. Liu, M.-M. Zhao, M. Lei, L. Li, Y. Cai, and M.-J. Zhao, "Adaptive HARQ Design for Semantic Image Transmission," in *2024 IEEE 100th Vehicular Technology Conference (VTC2024-Fall)*. IEEE, 2024, pp. 1–6.
- [15] N. Fei, L. Rongpeng, Z. Zhifeng, and Z. Honggang, "Topology data analysis-based error detection for semantic image transmission with incremental knowledge-based HARQ," *China Communications*, vol. 22, no. 1, pp. 235–255, 2025.
- [16] Y. Li, X. Wang, Z. Shi, and Y. Fu, "Semantic HARQ for Intelligent Transportation Systems: Joint Source-Channel Coding-Powered Reliable Retransmissions," *arXiv preprint arXiv:2504.14615*, 2025.
- [17] Y. Sheng, L. Liang, H. Ye, S. Jin, and G. Y. Li, "Semantic Communication for Cooperative Perception using HARQ," *IEEE Transactions on Cognitive Communications and Networking*, 2025.
- [18] S. Zhang, H. Huang, J. Liu, and H. Li, "Spelling error correction with soft-masked BERT," *arXiv preprint arXiv:2005.07421*, 2020.
- [19] T. Wu, Z. Chen, D. He, L. Qian, Y. Xu, M. Tao, and W. Zhang, "CDDM: Channel denoising diffusion models for wireless semantic communications," *IEEE Transactions on Wireless Communications*, vol. 23, no. 9, pp. 11 168–11 183, 2024.
- [20] J. Song, C. Meng, and S. Ermon, "Denosing diffusion implicit models," *arXiv preprint arXiv:2010.02502*, 2020.
- [21] C.-Y. Lin, "Rouge: A package for automatic evaluation of summaries," in *Text summarization branches out*, 2004, pp. 74–81.